On the origin of magnetoresistance in Sr_2FeMoO_6

D.D. Sarma* and Sugata Ray
Solid State and Structural Chemistry Unit, Indian Institute of Science, Bangalore 560 012, INDIA

K. Tanaka and A. Fujimori
Department of Physics and Department of Complexity Science and Engineering, University of Tokyo, Bunkyo-ku, Tokyo 113-0033, Japan

We report detailed magnetization (M) and magnetoresistance (MR) studies on a series of Sr_2FeMoO_6 samples with independent control on anti-site defect and grain boundary densities. These results, exhibiting a switching-like behavior of MR with M, establish that the MR is controlled by the magnetic polarization of grain boundary regions, rather than of the grains within a resonant tunnelling mechanism.

PACS number(s): 75.47.Gk, 72.25.-b, 75.60.-d

While colossal magnetoresistance (CMR) in manganites [1] spurted a tremendous level of research activities in view of its immense technological possibilities, the actual realization of any device application has been mainly impeded by the requirement of a low temperature and high magnetic field for an appreciable MR to be observed in these compounds. It has been demonstrated [2,3] that substantial negative MR can be achieved at reasonably low applied fields by specific grain boundary engineering; however, the requirement of a low temperature is still not conducive to wide-spread device applications. Thus, a great deal of interest has naturally been generated with the more recent discovery of CMR in polycrystalline Sr_2FeMoO_6 at a considerably higher temperature and lower magnetic field [4]. Magnetic scattering at magnetic domain boundaries can be ruled out as the origin of MR in this compound, because no significant MR was observed in the single crystalline compound [5], where magnetic domain boundaries exist. While all observations clearly suggest tunnelling magnetoresistance (TMR) to be the dominant cause of the CMR in Sr_2FeMoO_6, there is no clear agreement or understanding of the nature of tunnelling barriers in this system. Since, a proper identification of the primary mechanism for MR in this compound is essential as a first step towards realizing any useful application, we have carried out specific experiments to address this issue.

Two alternative origins of MR in Sr_2FeMoO_6 have been discussed so far. In one view, the physical grain boundaries are believed to provide tunnel barriers. But, another source of such tunnel barriers in this compound, arising from Fe/Mo antisite disorder giving rise to antiferromagnetic, insulating Fe-O-Fe patches in between fully-ordered metallic Sr_2FeMoO_6 islands within a single grain, has also been convincingly put forward [6]. Therefore, in this limit, the grain size of the polycrystalline sample will not affect the TMR significantly [6]. Various synthetic parameters [7], such as the annealing temperature, provide a useful handle to change the Fe/Mo sublattice ordering, thereby changing the density of antisite defects and the magnetization in a systematic way. Unfortunately, these synthetic processes also change the grain sizes (and thus the grain boundary density), the average thickness of the grain boundaries and also possibly the chemical composition of the grain boundaries (depending on the oxygen partial pressure and temper-

ature) in an uncontrolled manner. Here, we propose a route that allows us to control the two crucial parameters, namely the extent of ordering controlling the antisite defect density and the grain size determining the grain boundary density, independent of each other and keeping other physical properties essentially unchanged, thereby providing a critical test for the dominant mechanism of MR in Sr_2FeMoO_6. By varying these two control parameters independently, we show that the origin and behavior of the magnetoresistance is unique in this compound compared to all other systems.

All the Sr_2FeMoO_6 samples, studied here were first prepared by the arc melting method, leading to highly disordered samples, as characterized by x-ray diffraction (XRD) [8]. However, it produces samples (labelled A) with large grains (10-20 μm) and relatively few grain boundaries, as confirmed by scanning electron microscopy (SEM). We also prepared three other samples, B, C and D, by annealing A at 1173 K, 1523 K and 1673 K, respectively, for a period of 5 hours. SEM in conjunction with energy dispersive analysis of x-ray (EDX) revealed no change in the grain morphologies and composition due to this annealing process. The extent of the Fe/Mo ordering or the anti-site defect density, quantified by the intensity of the supercell (111) reflection at 19.6° normalized by the normal reflection at 32.1° ($I_{19.6^\circ}/I_{32.1^\circ}$) [4,8], increased progressively for A, B, D, C. ($I_{19.6^\circ}/I_{32.1^\circ}$) for sample C turns out to be larger than those previously prepared; consequently this sample has one of the largest saturation magnetization (3.54 μ_B/f.u.) reported in bulk Sr_2FeMoO_6 samples so far [6]. Then, we take approximately half of each of these four samples and grind them to a fine particle size with an average grain size of 2-3 μm and pelletize these at room temperature to form samples E, F, G and H from samples A, B, C, and D, respectively. Each pair of samples, namely (A, E), (B, F), (C, G) and (D, H) thus have the same antisite defect density within a group, but very different grain sizes and grain boundary density.

In Fig. 1a we show the $M(H)$ plots (solid lines) for the large grain samples, A-D, while for the small grain samples, we plot -$M(H)$ in order to avoid crowding together of the data, measured at 5 K. The saturation magnetizations of these samples increase monotonically with the extent of Fe/Mo ordering, possibly suggesting that antisite defects produce antiferromagnetic regions [6]. Inset to Fig. 1b shows a typical change in the resistivity (ρ) behavior as a function of temperature (T) within a pair of samples with the same antisite defect density but different grain sizes. The resistivity of the large grain sample is obviously metallic, being qualitatively and quantitatively similar to that of the single crystal samples [5]. In contrast, the corresponding small grain sample exhibits an insulating behavior with a resistivity that is at least four orders of magnitude larger compared to the large grain sample at all temperatures. Thus, it is clear that grain boundaries offer insulating barrier to macroscopic charge transport in these samples. Figure 1b shows the % MR (=100×[$R(H,$ T)-$R(0,$ T)]/$R(0,$ T)) for each of the compounds at 20 K. For the purpose of clarity and easy comparison, we show the % $MR(H)$ plot of the big grain samples A-D, for the negative sweep of the magnetic field, while the % $MR(H)$ for the small grain samples are shown for the positive sweep of the applied field. The intrinsically more noisy nature of MR in the large grain samples arises from the very low resistance of these samples (see inset) and a small $\Delta R = R(H) - R(0)$. It is quite clear that the % MR exhibited by the small grain samples are uniformly several times larger than those of the corresponding large grain samples. If we take into account the fact that the resistivities of the small grain samples are at least four orders of magnitude larger than that of the corresponding large grain samples with identical anti-site defect density, it becomes evident, that the absolute change in resistivity, ΔR, for the small grain sample is about five orders of magnitude larger than that from large grain samples of similar dimensions on application of the same magnetic field. These facts clearly establish that the predominant contribution to the observed MR in these samples arises from grain boundary effects, rather than from antisite defects.

In order to quantify the comparisons, we plot the % MR at 20 K and 1 T as a function of the ordering in Fig. 2. Since the extent of ordering is a direct measure of the antisite defect density, Fig. 2, evidently showing a very large enhancement (typically 100-200 %) of MR for the small grain samples compared to the large grain ones at about the same level of ordering, clearly establishes the grain boundaries instead of the antisite defects as the primary source for the dominant mechanism of MR in Sr_2FeMoO_6. Interestingly, there is a small increase in MR of sample D compared to sample C, though the extent of ordering as well as the saturation magnetization (see Fig. 1a) are lower for the sample D. In these large grain, molten ingots, the effect of grain boundaries is expected to be minimized, thereby enhancing the chances of observing small contributions from other effects, such as that of antisite defects. It is indeed true that the antisite defect density is much larger in sample D compared to C, owing to a lower Fe/Mo ordering; therefore, the small increase in MR observed between samples C and D suggests a small, but finite contribution to MR from such antisite defects, while the predominant part of the MR in all samples arises from the grain boundary effects. A similar argument would suggest a higher MR for sample B compared to that of D and the highest MR in A among the large grain samples due to a systematic increase of antisite defects, in sharp contrast to the experimental results (Fig. 2). This suggests that excessive introduction of antisite defects has an adverse effect on the MR, most likely arising from a marked reduction of the magnetic polarization of the bulk and hence the spin

polarization at E_F [9].

In order to understand the nature of MR in these compounds, we plot the % MR as a function of M/M_s in Fig. 3; the results for the corresponding pairs (A, E), (B, F), (C, G) and (D, H) are shown in different panels. These plots make a number of interesting behavior obvious. Evidently, the % MR does not exhibit the expected $(M/M_s)^2$ [10] behavior of a tunnelling barrier, except for the lowest MR (% $MR \leq 1\%$) regime in the large grain sample, A-D, as shown more clearly in the insets with % MR plotted against $(M/M_s)^2$, also illustrated by overlapping the best fit $(M/M_s)^2$ function (dotted line) on the experimental plots in the main frames of Fig. 3. Manifestation of the $(M/M_s)^2$ behavior for the initial ($\leq 1\%$) MR specifically in the large grain samples, with significantly reduced grain boundary effects, suggests that the tunnelling barriers are possibly provided for these samples by the previously discussed antisite defect boundaries [6]. The remaining and the larger part of the MR, therefore, arises from intergrain effects. However, this intergrain tunnelling contribution evidently does not have the expected $(M/M_s)^2$ dependence and intriguingly almost switches on (signalled by the very rapid increase) at a substantially large value of (M/M_s) in every case, though more pronounced in the highly ordered small grain samples. For example, sample G with the maximum MR value (see Fig. 3c) exhibits only about 6 % MR for $(M/M_s) = 0.9$, the remaining nearly 18 % MR is achieved with the magnetization achieving the last 10 % of its saturation value. Though much attention has been focussed on the *l*ow-field MR in Sr_2FeMoO_6, in view of the results in Fig. 3 and the above discussion, it appears that Sr_2FeMoO_6 in fact requires an unusually large field to realize the MR in the sense that an applied field, though enough to reach 50-80 % of the saturation magnetization, is not enough to show more than 1 % MR. These observations clearly suggest that the dominant origin of MR in Sr_2FeMoO_6 cannot be understood in terms of the usual TMR scenario with electron transport across an inert tunnelling barrier by aligning the magnetization of the two grains across the grain boundary by the application of a magnetic field. It appears to be necessary to magnetize and therefore magnetically align the grain boundary itself in order to achieve the MR response, suggesting the switching-on of a resonant tunnelling mechanism in the grain boundary magnetization, rendering the % MR relatively insensitive to the extent of bulk magnetization, (M/M_s). From the low-field value of $(M/M_s) \sim 0.9$, it seems that roughly about 10 % of the total magnetization in the high field comes from the magnetic nature of the grain boundary. A final evidence for these suggestions comes from the following observation.

The MR plots for the small grain samples consistently exhibit a sizable hysteresis in the low field (≤ 1 T) regime, while that of the large grain samples do not exhibit any noticeable hysteresis (see Fig. 1b and 3). The near absence of hysteresis in the large grain samples is consistent with the near absence of any hysteresis in the corresponding magnetization plots in Fig. 1a. It has been found for all oxide systems, such as for CrO_2 in ref. [12], for manganites in ref. [13], as well as for Co-Cu alloys in ref. [14] that the peak in MR coincides with the corresponding coercive fields (H_c), as should indeed be expected for TMR. In order to carefully compare the hysteresis in MR and M in small grain samples, we show MR and M as function of H on an expanded scale ($|H| \leq 0.3$ T), in Fig. 4. The figure clearly shows the hysteresis loops in M vs. H as well as in MR vs. H. In striking contrast to other systems [11–13], small grain Sr_2FeMoO_6 intriguingly shows a peak in MR at an H about 6 times larger than H_c. This is possible only if the grain boundary region controlling the TMR in this material has a much larger coercive field than H_c of the bulk, while the intragrain properties dominate the $M(H)$ behavior. This suggestion is consistent with all the observations presented here so far. Additionally this is further supported by a small but definite increase in the coercive fields of the small grain samples compared to the large grain ones, due to the presence of large number of grain boundaries with much higher H_c in the small grain samples, as illustrated for the (D, H) pair in the inset of Fig. 4.

In conclusion, by controlling independently the antisite defect density and grain boundary density in a series of Sr_2FeMoO_6 samples, we show that the MR originates primarily from tunnelling across the grain boundaries, with very small contributions from anti-site defects. This TMR from the grain boundaries exhibits several intriguing features, most notably (i) a switching-like behavior of MR, and (ii) the peak in $MR(H)$ appearing at an H several times higher than the H_c seen in $M(H)$ curves. These are explained in terms of the different, specifically harder, magnetic nature of the grain boundary region compared to the bulk, controlling the resonant tunnelling behavior and thereby the MR, instead of providing a simple tunnelling barrier.

We thank A. Fujiwara for help in the SQUID measurements. DDS thanks university of Tokyo for hospitality during a part of this work.

⋆ Also at Jawaharlal Nehru Centre for Advanced Scientific Research, Bangalore, India. sarma@sscu.iisc.ernet.in

[1] For reviews, see Colossal Magnetoresistive Oxides, edited by Y. Tokura (Gordon and Breach, London, 1999).
[2] N.D. Mathur *et al.*, Nature **387**, 266 (1997).
[3] A. Gupta *et al.*, Phys. Rev. B **54**, R15629 (1996).
[4] K. -I. Kobayashi *et al.*, Nature **395**, 677 (1998).
[5] Y. Tomioka *et al.*, Phys. Rev. B **61**, 422 (2000).

[6] M. Garcia-Hernandez *et al.*, Phys. Rev. Lett. **86**, 2443 (2001).
[7] Ll. Balcells *et al.*, Appl. Phys. Lett. **78**, 781 (2001).
[8] D. D. Sarma *et al.*, Solid State Commun. **114**, 465 (2000).
[9] T. Saha-Dasgupta and D.D. Sarma, Phys. Rev. B **64**, 064408 (2001).
[10] Pinaki Majumdar and Peter B. Littlewood, Nature **395**, 479 (1998).
[11] J. M. D. Coey *et al.*, Phys. Rev. Lett **80**, 3815 (1998).
[12] X. W. Li, A. Gupta, G. Xiao and G. Q. Gong, Appl. Phys. Lett. **71**, 1124 (1997).
[13] J. Q. Xiao, J. S. Jiang and C. L. Chien, Phys. Rev. Lett. **68**, 3749 (1992).

FIG. 1. (a) $M(H)$ plots (solid lines) and -$M(H)$ plots (dashed lines) for the large and small grain samples, respectively. (b) % $MR(H)$ are shown for the large grain samples (solid circles) on the left half and for the small grain samples (lines) on the right half. The inset shows the typical changes in the resistivity with temperature between a large and a small grain samples with the same level of anti-site defect densities.

FIG. 2. Variation of % MR at 1T with the extent of ordering in the sample, as measured by the normalized intensity of the supercell reflection at 19.6°.

FIG. 3. The dependence of % MR on M/M_s for various samples. Each of the four panels compare the % MR obtained for a pair of large and small grain samples with the same anti-site defect density. The insets show the % MR as a function of the $(M/M_s)^2$ for the corresponding large grain samples, with the best-fits to $(M/M_s)^2$ dependence, expected theoretically, shown by the solid lines in the inset and the dashed lines in the main frame.

FIG. 4. A comparison between the low-field region of the MR and M in one illustrative case. The inset shows the comparison of $M(H)$ for a typical large and small grain samples.

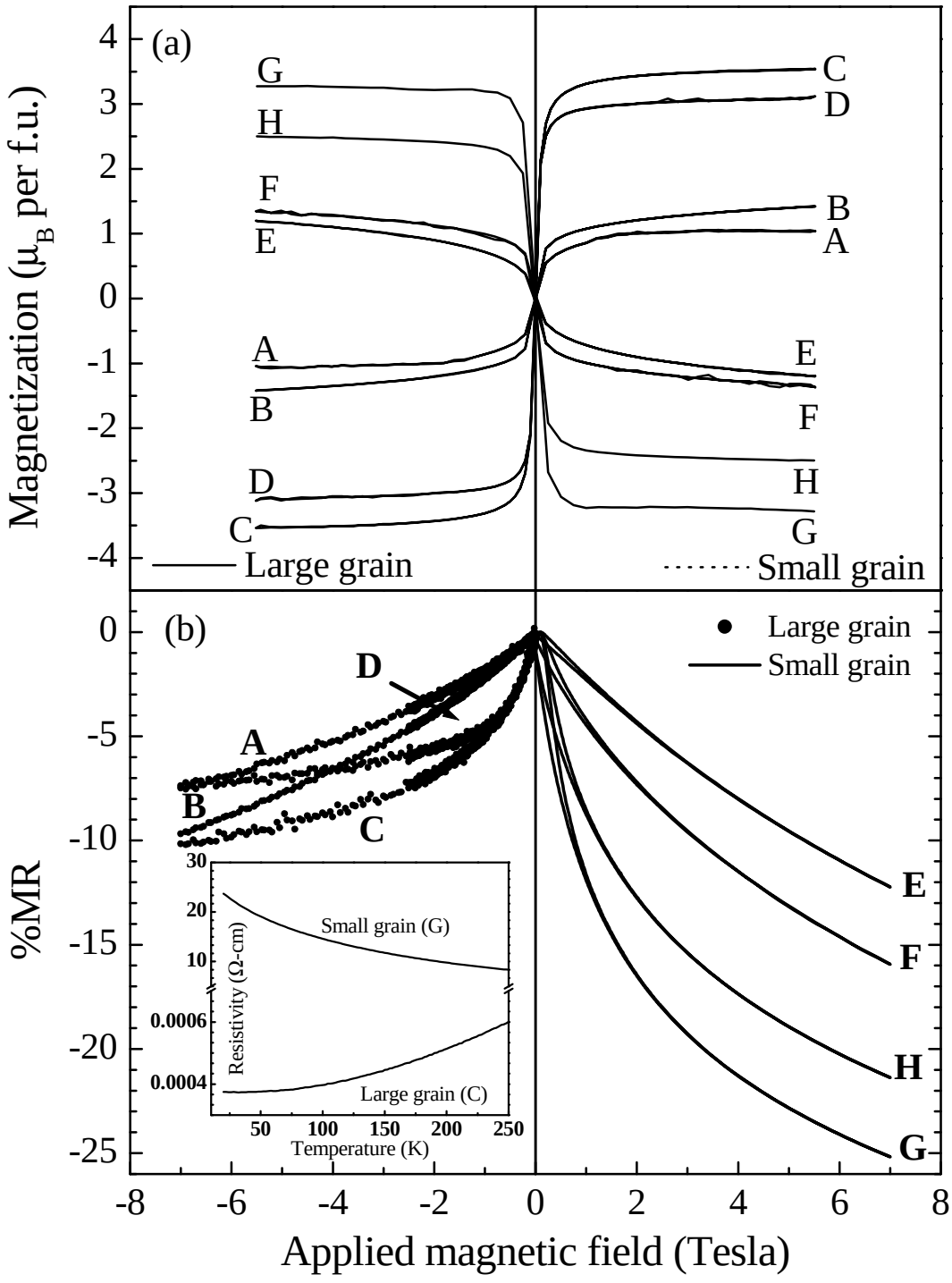

Fig. 1
Sarma *et al.*

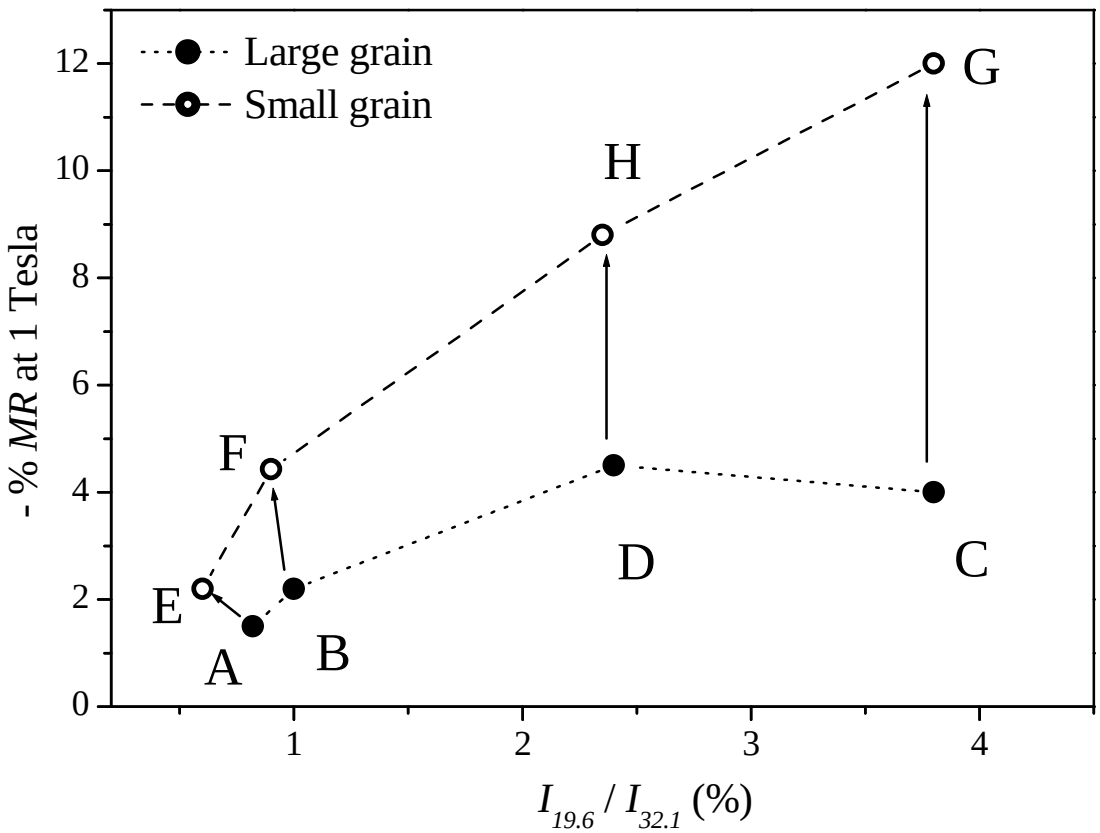

Fig. 2
Sarma *et al.*


This figure "Fig3_MR_condmat.jpg" is available in "jpg" format from:
http://lanl.arXiv.org/ps/cond-mat/0311013

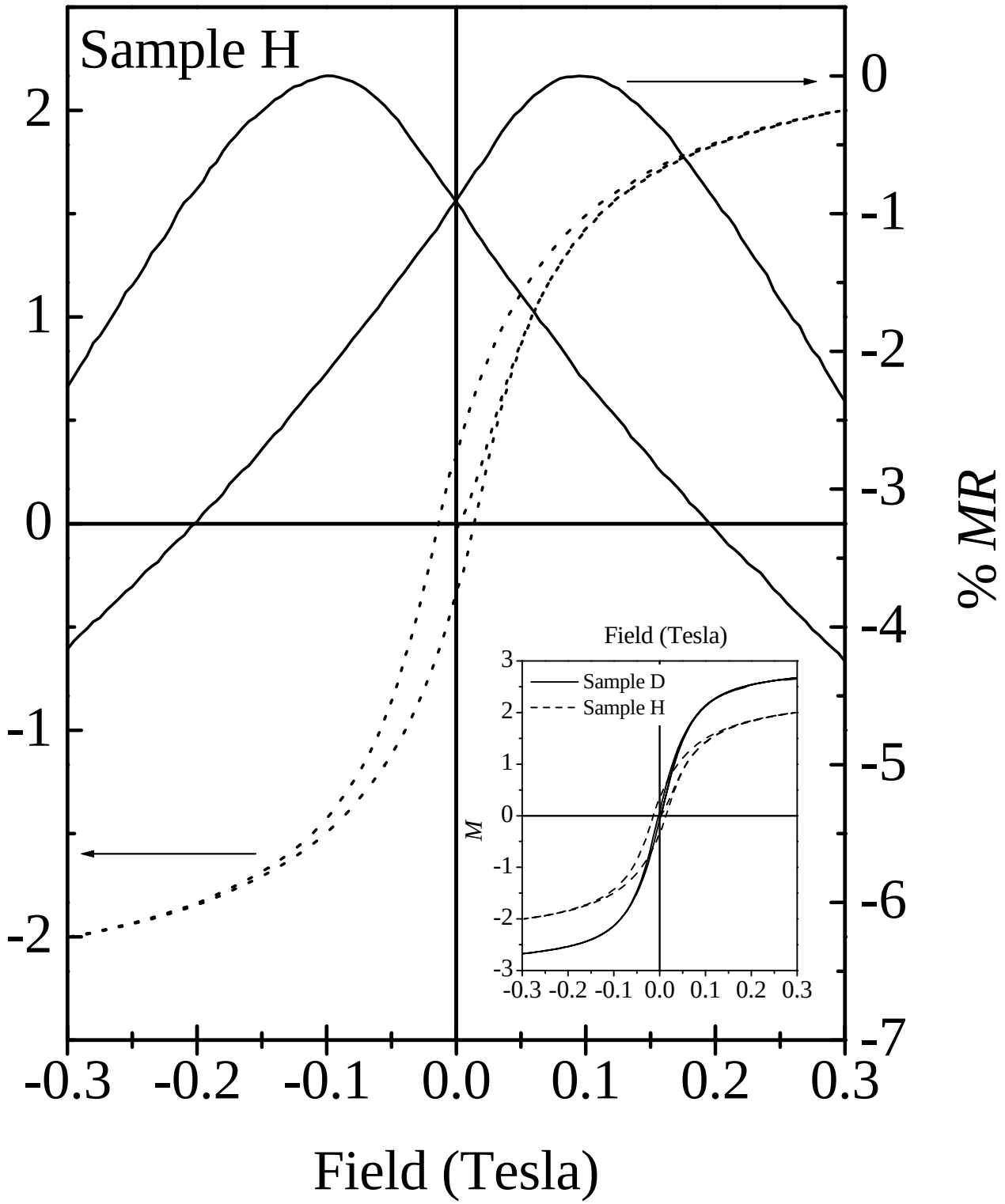

Fig. 4
Sarma *et al.*